Refractive index dependence of the coupling characteristics between long-range surface-plasmon-polariton and dielectric waveguide modes

Fang Liu,[1,2] Ruiyuan Wan,[1] Yidong Huang,[1,3] and Jiangde Peng[1]

[1]*State Key Laboratory of Integrated Optoelectronics, Department of Electronic Engineering, Tsinghua University, Beijing 100084, China*

[2] *liu_fang@tsinghua.edu.cn*

[3] *yidonghuang@tsinghua.edu.cn*

Received March 24, 2009; revised July 24, 2009; accepted July 27, 2009; posted August 17, 2009 (Doc. ID 109164); published August 31, 2009

The coupling characteristics of a hybrid coupler comprised of a long-range surface-plasmon-polariton (LRSPP) waveguide and a dielectric waveguide is analyzed with different detecting layers. Calculation results show that the coupling strength between the LRSPP mode and the dielectric-waveguide mode is rather sensitive to the refractive index of the detecting layer. This is promising to realize an integrated refractive index senor with high resolution better than 4×10^{-7} refractive index units or a modulator with rather low driving power and insert loss. © 2009 Optical Society of America

OCIS codes: 240.6680, 280.4788, 230.4110.

A surface-plasmon polariton (SPP) is a kind of TM surface electromagnetic excitation that propagates in a wavelike fashion along the interface between metal and dielectric media [1]. As a kind of special surface wave, the SPP has been used in biosensors [2] and shows potential for new type integrated optical devices [3,4]. The long-range SPP (LRSPP) mode is a kind of low-loss and dielectric refractive-index-sensitive SPP mode [5], and the LRSPP-based modulator [6] and sensor [7] have been studied.

Our group has reported a kind of hybrid coupler composed of an LRSPP waveguide and a dielectric waveguide and demonstrated the coupling between these two different modes [8]. This hybrid coupler not only can be used as a functional optical device but also provides a new approach to link the SPP devices and the dielectric devices. In this Letter, the coupling characteristics for the hybrid coupler with up–down structure are analyzed. It is found that the coupling strength is very sensitive to the refractive index of the dielectrics on the metal. When this structure is applied as the refractive index sensor, its resolution can be better than 4×10^{-7} refractive index units (RIU), which is 1 order of magnitude higher than the conventional waveguide sensor [2]. Furthermore, thanks to the high sensitivity to the refractive index, a kind of modulator with ultralow electric driving power can also be realized.

For simulation, a 1D structure is considered here and is shown in Fig. 1. The wavelength is fixed at $\lambda_0=1.55$ μm, and z is the propagation direction. Above the SiO_2 substrate ($n_s=1.444$ [9]) is the up–down hybrid coupler structure, which consists of the single-mode dielectric waveguide (light gray layer with $n_d=2.0$ and $T_d=52$ nm), the dielectric buffer layer ($n_{buff}=1.444$, $D=7$ μm), the metal LRSPP waveguide (dark gray layer with $T_m=30$ nm), and the detecting layer ($T_{det}=3$ μm) with changeable refractive index n_{det}. Above the detecting layer is the air ($n_c=1$) layer. Here, in spite of the relative high loss, Al with dielectric constant $\varepsilon_m=-252.48+i\times46.078$ [9] is selected instead of Au. The reason will be discussed later in this Letter. The length of the coupling region (length of the metal) is L.

For the hybrid coupler mentioned above, the coupling performances should be closely related to the characteristics of the LRSPP mode, including field distribution, propagation constant, and loss, which are sensitive to the refractive index difference between the substrate and the superstrate [10]. Therefore a slight refractive index change of the detecting layer would notably influence the coupling efficiency between the LRSPP and the dielectric waveguide mode. This can be illustrated by calculating the coupled eigenmodes, the energy coupling efficiency, and the coupler output power of the structures with different detecting layers.

First of all, the eigenmodes of the hybrid coupler ($0<z<L$) are calculated by adopting the transfer matrix method [11]. Figure 2 shows the real part (the imaginary part is much smaller and is not shown here) of the magnetic field $\boldsymbol{H}_j$ with a different detect-

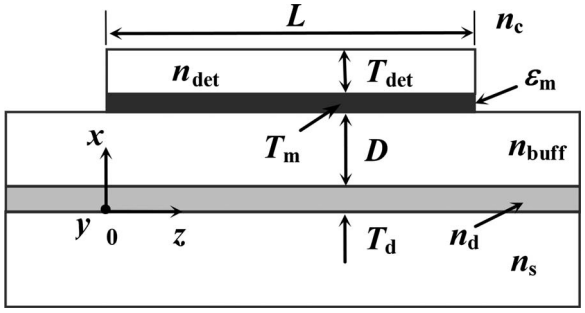

Fig. 1. Hybrid coupler structure with a dielectric waveguide (light gray layer), a metal LRSPP waveguide (dark gray layer), and a dielectric detecting layer on the metal.

0146-9592/09/172697-3/$15.00

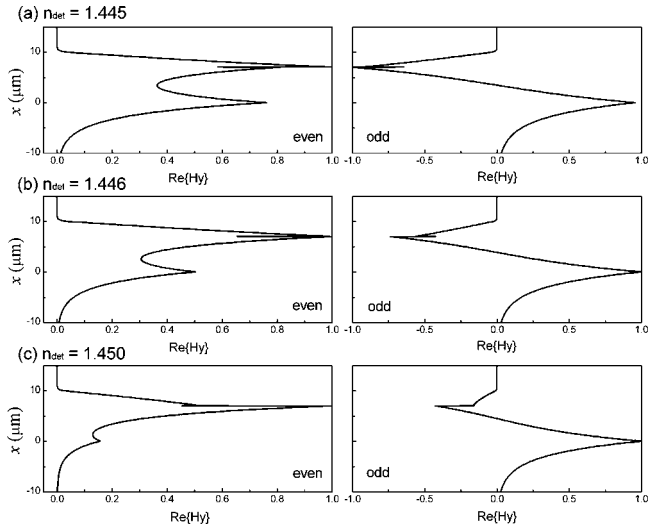

Fig. 2. Magnetic field distribution Re$\{H_y\}$ of even and odd eigenmodes with different n_{det}.

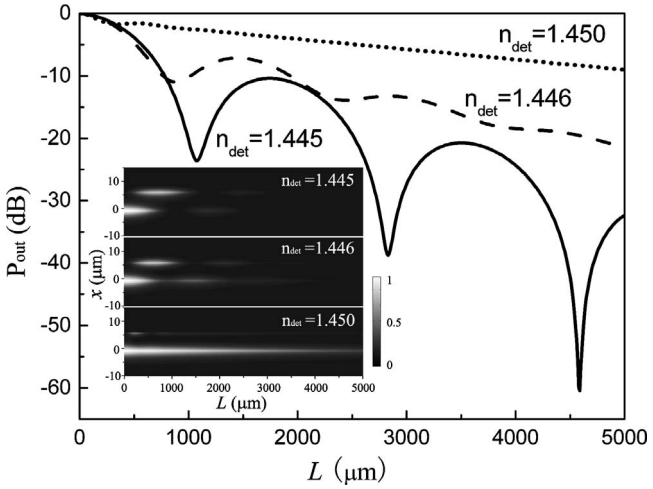

Fig. 3. Output power from dielectric waveguide P_{out} versus L in circumstances of different n_{det} when the input is applied on the dielectric waveguide. Inset, corresponding field intensity.

ing layer. When $n_{\mathrm{det}}=1.445$, the two eigenmodes have the almost symmetric and antisymmetric field distribution, as shown in Fig. 2(a). When $n_{\mathrm{det}}=1.446$, the field distribution shown in Fig. 2(b) is obviously unsymmetric. Further increasing n_{det} to 1.450, the two eigenmodes present a severe unsymmetric distribution, as shown in Fig. 2(c).

Expanding the TM mode ($0<z<L$) by the eigenmodes $\boldsymbol{H}_{\mathrm{j}}$ (even and odd eigenmodes), one gets

$$\boldsymbol{H}(x,y,z)=\sum_j a_j\boldsymbol{H}_j(x,y)e^{i\beta_j z}, \tag{1}$$

where β_{j} and a_{j} are the complex propagation constant and the mode constant, respectively. With normalized fields for all modes in unconjugated form [12,13], a_j can be derived from

$$a_j=\frac{1}{2}\int(\boldsymbol{E}_d\times\boldsymbol{H}_j)\cdot\hat{z}\,\mathrm{d}x, \tag{2}$$

with the TM mode $\boldsymbol{E}_{\mathrm{d}}$ of the dielectric waveguide as the input at $z=0$. The output power P_{out} from the dielectric waveguide can be obtained by

$$\begin{aligned}P_{\mathrm{out}}&=20\times\lg\left\{\left|\frac{1}{2}\int\boldsymbol{E}_{\mathrm{d}}\times\left[\sum_j a_j\boldsymbol{H}_j(x,y)e^{i\beta_j L}\right]\cdot\hat{z}\,\mathrm{d}x\right|\right\}\\&=20\times\lg\left(\left|\sum_j a_j^2 e^{i\beta_j L}\right|\right).\end{aligned} \tag{3}$$

According to Eqs. (1) and (2), the field intensity $|\boldsymbol{H}|^2$ propagating along z direction can be obtained and is shown as the inset of Fig. 3. When $n_{\mathrm{det}}=1.445$, the energy couples completely from the dielectric arm to the metal arm then returns to the dielectric arm again. The complete energy exchange results in large power loss because of the high-loss metal. When $n_{\mathrm{det}}=1.446$, it is a partial energy exchange, and there is always some energy remaining in the dielectric arm. This can be revealed by the obvious unsymmetric eigenmodes shown in Fig. 2(b), just like those in the conventional dielectric coupler [14]. In this case, since less energy couples to the metal arm, the total power loss along the z direction is lower. When $n_{\mathrm{det}}=1.450$, almost no coupling happens and the energy nearly passes directly through the dielectric arm with the lowest loss.

Having known the field intensity propagating along z, the curves of P_{out} shown in Fig. 3 can be understood easily. The ripple of the curve is due to the energy exchange between the dielectric and metal arms, and the depth of the ripple indicates the extent of the energy exchange. In these three curves, the solid curve ($n_{\mathrm{det}}=1.445$) has the deepest ripple, which indicates the complete energy exchange. Considering that the loss of the coupler is decided by the proportion of the energy coupled to the high-loss metal arm, it is easy to understand why the solid curve with larger ripple decreases much more quickly than the other two curves.

The above results shown in Fig. 2 and 3 indicate that the tiny shift of the n_{det} would affect the symmetry of the eigenmodes, the coupling efficiency, and the output power from the dielectric arm. Therefore, for the devices with fixed L, the output power P_{out} changes dramatically with n_{det}, as shown in Fig. 4. The solid curve corresponds to the local minimum of the solid curve in Fig. 3 ($L=2830$ μm). Surrounding $n_{\mathrm{det}}=1.445$, even 10^{-3} shift of n_{det} would result in 20 dB output power change. Therefore the structure shown in Fig. 1 can be applied as a kind of sensor to detect the refractive index change Δn_{det}. Compared with the results in [15], the width of the curve in Fig. 4 is much narrower, which means much higher sensitivity. The resolution (sensitivity) of the sensor can be estimated by

$$\mathrm{Resolution}=\frac{f_{\mathrm{pm}}}{\mathrm{Sensitivity}}=f_{\mathrm{pm}}\times\frac{\Delta n_{\mathrm{det}}}{\Delta P_{\mathrm{out}}}, \tag{4}$$

where f_{pm} (assumed as 0.01 dB here [2]) is the resolution of the power meter. For the solid curve in Fig. 4, the average resolution between 1.444 and

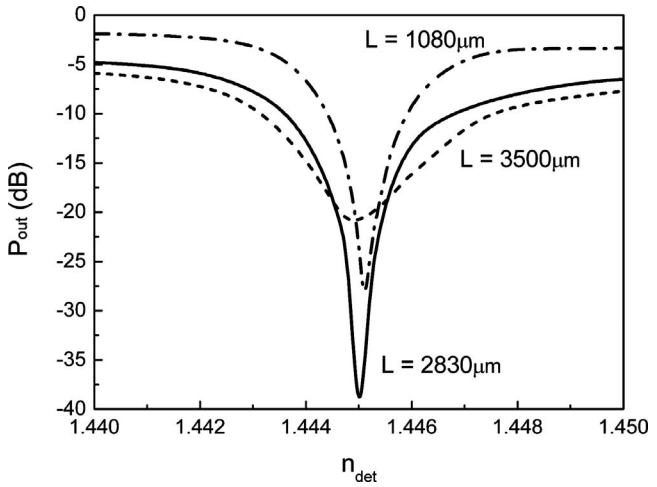

Fig. 4. Output power from dielectric waveguide P_{out} as a function of n_{det} with different L.

1.446 is 4×10^{-7} RIU, according to Eq. (4), which is 1 order of magnitude better than the traditional waveguide-based surface-plasmon sensor [2].

Sometimes the coupling length L may not just correspond to the local minimum of the solid curve in Fig. 3. The worst situation is that L happens to be located at the local maximum of the curve ($L=3500\ \mu$m), which indicates that all of the energy couples back from metal waveguide to the dielectric waveguide. The corresponding P_{out} versus n_{det} is shown as the dashed curve in Fig. 4. Although the resolution decreases, rather high resolution 2×10^{-6} RIU can still be obtained when n_{det} is between 1.443 and 1.447. Having known the coupling characteristics with different detecting layer, it should be easy to understand that the resolution (sensitivity) of this worst situation is decided by the loss of the LRSPP mode. Reducing the loss of metal can reduce the difference of the overall slope of the curves in Fig. 3 effectively. Then the local maximum points of the three curves would be very close to each other and result in lower resolution when L happens to be the worst situation. Therefore to increase the fabrication tolerance of L, metal with relatively high loss, such as Al, is selected.

This hybrid coupler structure can also be applied as an optical intensity modulator by actively changing n_{det}. Selecting $L=1080\ \mu$m, the output power P_{out} versus n_{det} is shown as the dashed-dotted curve in Fig. 4. Adopting electro-optical material as the detecting layer, the voltage modulation signal can be transferred to the variation of n_{det} then to the P_{out}. The modulation voltage can be very low, thanks to the highly sensitive P_{out} to n_{det} and very thin dielectric detecting layer. Moreover, the insert loss is as low as −2 dB when n_{det} is far from 1.445.

In conclusion, the coupling characteristics between the LRSPP mode and the dielectric-waveguide mode are analyzed. It is found that the coupling between these two different kinds of modes is rather sensitive to the refractive index of the dielectric detecting layer on the metal surface. This kind of hybrid coupler structure can be applied as a refractive index senor with resolution as high as 4×10^{-7} RIU. Furthermore, it is also promising to realize an intensity modulator with ultralow driving power.

This work is supported by the National Basic Research Program of China (973 Program) under contract 2007CB307004 and the National Natural Science Foundation of China (NSFC) (NSFC-60537010 and NSFC-60877023). The authors would like to thank Prof. Wei Zhang and Dr. Xue Feng of Tsinghua University and Mr. D. Ohnishi, Mr. D. Niwa, Mr. Y. Miura of ROHM Corporation for their valuable discussions and helpful comments.

References

1. H. Raether, *Surface Plasmons* (Springer-Verlag, 1988).
2. J. Homola, S. S. Yee, and G. Gauglitz, Sens. Actuators B **54**, 3 (1999).
3. R. Charbonneau, C. Scales, I. Breukelaar, S. Fafard, N. Lahoud, G. Mattiussi, and P. Berini, J. Lightwave Technol. **24**, 477 (2006).
4. A. Boltasseva, T. Nikolajsen, K. Leosson, K. Kjaer, M. S. Larsen, and S. I. Bozhevolnyi, J. Lightwave Technol. **23**, 413 (2005).
5. I. Breukelaar and P. Berini, J. Opt. Soc. Am. A **23**, 1971 (2006).
6. T. Nikolajsen, K. Leosson, and S. I. Bozhevolnyi, Appl. Phys. Lett. **85**, 5833 (2004).
7. G. G. Nenninger, P. Tobisika, J. Homola, and S. S. Yee, Sens. Actuators B **74**, 145 (2001).
8. F. Liu, Y. Rao, Y. Huang, W. Zhang, and J. Peng, Appl. Phys. Lett. **90**, 141101 (2007).
9. E. D. Palik, *Handbook of Optical Constants of Solids* (Academic, 1985).
10. I. Breukelaar, R. Charbonneau, and P. Berini, J. Appl. Phys. **100**, 043104 (2006).
11. C. Chen, P. Berini, D. Feng, S. Tanev, and V. Tzolov, Opt. Express **7**, 260 (2000).
12. A. W. Snyder and J. D. Love, *Optical Waveguide Theory* (Chapman, 1983), pp. 212–214.
13. R. Wan, F. Liu, X. Tang, Y. Huang, and J. Peng, Appl. Phys. Lett. **94**, 141104 (2009).
14. D. Marcuse, J. Lightwave Technol. **LT-5**, 113 (1987).
15. J. Ctyroký, J. Homola, P. V. Lambeck, S. Musa, H. J. W. M. Hoekstra, R. D. Harris, J. S. Wilkinson, B. Usievich, and N. M. Lyndin, Sens. Actuators B **54**, 66 (1999).